



Cite this: *Chem. Sci.*, 2019, **10**, 7988

All publication charges for this article have been paid for by the Royal Society of Chemistry

Received 3rd June 2019
Accepted 11th July 2019

DOI: 10.1039/c9sc02699a
rsc.li/chemical-science

Fluoro-electrochemical microscopy reveals group specific differential susceptibility of phytoplankton towards oxidative damage†

Minjun Yang, ^a Christopher Batchelor-McAuley, ^a Lifu Chen, ^a Yanjun Guo, ^a Qiong Zhang, ^b Rosalind E. M. Rickaby, ^b Heather A. Bouman ^b and Richard G. Compton ^{*a}

In the vicinity of an electrode creating a highly oxidising environment the fluorescence – arising from the presence of chlorophyll-a – of single cellular phytoplankton becomes inhibited. Even for phytoplankton that are very comparable in size (ca. 2–20 µm) the rate of this (electro)chemically induced fluorescence inhibition differs significantly between phytoplankton species; the fluorescence signal of the freshwater algae *Stichococcus bacillaris* turns off ~70 times faster than that of the marine coccolithophore *Emiliana huxleyi*. The varying behaviour reflects the differing susceptibility of these globally important phytoplankton species towards extreme levels of radical induced oxidative stress, indicating the physical and chemical properties of the plankton cell wall and membrane are very different between species, and are important in determining their susceptibility. These results have potential implications for the analytical detection and characterisation of phytoplankton cells in the natural environment.

Introduction

The denomination phytoplankton is a broad catch-all term encompassing a range of single cellular microorganisms spanning twelve taxonomic divisions and includes both Eukaryotes and Bacteria. Over 5000 species of phytoplankton¹ have been identified with sizes ranging from 1 µm to over 100 µm. However, all phytoplankton cells contain chlorophyll-a (chl-a) which absorbs light and is used for the conversion of dissolved inorganic carbon (e.g. CO_{2(aq)}) to organic molecules such as carbohydrates, lipids and proteins.² Although individual phytoplankton are microscopic in size, they are responsible for approximately half of the photosynthesis on Earth, and are the conduit through which energy enters aquatic ecosystems. There is currently active debate regarding the extent to which global phytoplankton biomass may have declined over the previous century;^{3,4} this has serious implications for the global marine ecosystem. Phytoplankton cells can achieve high densities in the natural environment that alter the colour of the surface ocean which can be viewed in satellite images.⁵ These images

can be used to remotely measure the scale and density of a phytoplankton bloom.^{6–8}

Beyond the use of chl-a fluorescence to estimate phytoplankton biomass, the time variation of the cellular chl-a fluorescence intensity may also be used to yield insight into the photosynthetic performance of phytoplankton.^{9,10} Fast repetition rate fluorometry¹¹ allows, amongst other parameters, the photochemical conversion efficiency and the photosystem II functional absorption cross section to be analysed. Such cell physiology measurements, in combination with the assessments of cell growth are a common route by which the effects of cellular oxidative stress are investigated.¹² In terms of species identification and cell density estimation, both at sea and in the laboratory, flow cytometry is a primary technique,¹³ where the relationship between side scatter *versus* fluorescence intensity is used to identify the presence of different plankton species. This procedure is however not without limitations; problems arise when species have similar optical properties or when single species display a wide size range due to cell agglomeration and chain formation.¹⁴

Reflecting the fact that phytoplankton occur in a number of taxonomic divisions, their composition, shape and size varies widely between species. For example *Emiliana huxleyi* is a representative species of calcifying phytoplankton; such plankton produce plates of calcium carbonate inside their cells which are extruded onto their external cell walls. These calcifying plankton species play a critical role in the oceanic carbon cycle.^{15–18} Despite being energetically costly,¹⁹ it has been proposed that calcification offers coccolithophores physical

^aPhysical and Theoretical Chemistry Laboratory, Department of Chemistry, University of Oxford, South Parks Road, Oxford, OX1 3QZ, UK. E-mail: Richard.Compton@chem.ox.ac.uk

^bDepartment of Earth Sciences, University of Oxford, South Parks Road, Oxford, OX1 3AN, UK

† Electronic supplementary information (ESI) available. See DOI: 10.1039/c9sc02699a

protection, reduces UV damage, and potentially accelerates photosynthesis.^{20,21} In contrast, diatoms are encased in a siliceous skeleton and play a key role in the transport of carbon to the ocean's interior. The morphologically diverse green algae are cosmopolitan members of aquatic ecosystems and can be important contributors to primary production in productive marine and freshwater environments.

In clear water solar UV radiation penetrates to a depth of 10–20 m.^{22,23} The susceptibility of phytoplankton towards solar radiation damage has been previously reported, where the sensitivity of different species is often interpreted on an allometric (cell size) basis.^{24,25} Beyond direct radiation damage, UV light is also able to photolyse nitrate, nitrites and other chromophoric dissolved organic matter present in the ocean; these photoreactions are a major source of hydroxyl radicals in the marine environment.²⁶ Furthermore, at the air–water interface the transfer of atmospheric hydroxyl radicals to the water has also been evidenced to be an important source of oxidising radicals.²⁷ Once transferred or formed in the aqueous phase these highly reactive hydroxyl radicals will lead to the formation of other reactive species such as carbonate radicals. Highly oxidising and reactive species are potentially deleterious for aquatic life.²⁸

Radical species can be formed not just photochemically but also electrochemically. Hydroxyl radicals can be generated on a large scale *via* a strong electric-field gas discharge (kV) to eliminate invasive marine species in ship's ballast water,²⁹ microscopic marine species such as phytoplankton and bacteria were shown to be killed within tens of seconds.^{30–33} On a small scale, high potentials at carbon electrodes can oxidise water and/or the ions present in solution ("solvent breakdown"). Although at these high potentials the formation of oxygen from water is thermodynamically favourable, the process involves multiple steps; consequently, in the absence of a suitable oxygen evolving catalyst such as a metal oxide,^{34,35} significant quantities of reactive intermediates (such as hydroxyl radicals, OH[·]) will be formed. At pH 7 the electrode potential for the one-electron oxidation of water to the hydroxyl radical is +2.07 V (vs. Saturated Calomel Electrode, SCE).³⁶ Hence, in accordance with the Nernst equation and assuming reversibility of the electrode process, the formation of concentrations of hydroxyl radicals as high as millimolar may be favourable at around ~1.9 V (vs. SCE). Notably, the direct one-electron oxidation of hydroxide occurs at significantly lower potentials of 1.3 V vs. SCE on gold electrodes.³⁷

This article studies the interaction between phytoplankton and electrochemically formed highly oxidising species using fluorescence electrochemical microscopy. We primarily focus on the study of six phytoplankton in four different groups, namely a diatom (*Halimphora coffeaeformis*), a coccolithophore (*Emiliana huxleyi*), the eustigmatophyte *Nannochloropsis oceanica* and three fresh water green algae (*Stichococcus bacillaris*, *Chlorella singularis* and *Chlorella volutis*). Also investigated is a representative dinoflagellate (*Scrippsiella trochoidea*), however, study of this species was somewhat limited by its low cell density. The results evidence the widely different sensitivity of phytoplankton species towards strongly oxidising

environments, and indicate that the differences reflect the different physical and chemical composition of the shells and outer membranes of the phytoplankton.

Results and discussion

All species selected for study in this work are comparable in size with length scales in the range of 2–20 μ m. The plankton can be visualised under a fluorescence microscope (excitation wavelength of 475 ± 35 nm and the emission by-pass above >590 nm) due to their strong fluorescence response arising from the presence of chl-a in the cells. However, these species differ markedly in their cell structure, the diatom has a porous silicate shell, the coccolithophore can be found encased in a shell of calcium carbonate and the algae have cellulose based cell walls (see ESI† Section 1 for further information).

This work starts by studying the response of the diatom *H. coffeaeformis* in a fluoro-electrochemical cell. Fig. 1 depicts a series of fluorescent microscope images for *H. coffeaeformis*. The bright features present in the optical field are the phytoplankton present either as individuals or in larger agglomerates. These diatoms are held in a thin layer cell (*ca.* 50 μ m depth) which also contains a carbon fibre electrode (electrode radius = 3.5 μ m). The cell also contains counter and reference electrodes. A schematic of the cell is shown in the ESI† Section 2 along with full experimental details. These carbon fibre electrodes are non-fluorescent and hence are not observable under the epi-fluorescent illumination conditions. In Fig. 1 the position of the carbon fibre wire is indicated by the blue line across the microscope image. Initially a potential of 0.0 V was initially applied to the electrode for 60 s and a series of microscope images recorded at 10 frames per second. At this potential (0.0 V) no Faradaic reactions occur at the carbon fibre electrode. After 60 seconds the applied potential is stepped to an oxidative potential of +2.3 V. Fig. 1 shows a series of images of the thin-layer cell taken at different times after the onset of the higher potential (the full Video can be found in ESI† Section 3). As can be seen from Fig. 1 the fluorescence response of *H. coffeaeformis* closest to the electrode are 'switched off' first and the fluorescence associated with the diatoms further away from the electrode progressively decrease with increasing time. First, a potential above approximately +1.4 V (see ESI† Section 4)

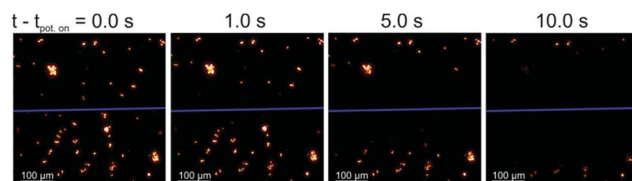


Fig. 1 Optical images of the chl-a fluorescence of *H. coffeaeformis* (diatom, CCAP 1001/2) during the fluoro-electrochemical experiment, where $t_{\text{pot. on}}$ is the time which a potential step of 2.3 V (vs. pseudo Ag wire) was applied to the working electrode. $\lambda_{\text{ex}} = 475 \pm 35$ nm and $\lambda_{\text{em}} > 590$ nm. The blue line depicts the location of the carbon fibre electrode. A potential of 0 V (vs. pseudo Ag wire) was applied for $t = 0$ –60 s, before the potential steps to 2.3 V for $t = 60$ –90 s.



needs to be applied to the electrode in order for the fluorescence of the phytoplankton to be affected over the timescale of the experiment (*ca.* tens of seconds). Second, no change in the fluorescence response of the diatoms was observed if a reductive potential was held on the electrode (studied down to -2.0 V). The following section serves to quantify the rate at which this electrochemically induced change in cellular fluorescence occurs.

The fluorescence response of individual phytoplankton were measured over the entire plankton cell *via* integration of the microscope image to obtain per plankton mean fluorescence intensities. The perpendicular distances between different plankton and the electrode were also measured and found to be in the range of $2\text{ }\mu\text{m}$ to $330\text{ }\mu\text{m}$. Fig. 2 shows the integrated fluorescence intensity of five individual and representative *H. coffeeaeformis* cells as a function of time, the fluorescence intensity has been normalised against its value recorded at $t - t_{\text{pot-on}} = 0\text{ s}$ and each trace in Fig. 2 is for a different diatom. The fluorescent transients depicted in Fig. 2 are for diatoms situated in the range of $10\text{--}250\text{ }\mu\text{m}$ away from the carbon electrode. As can be seen, the mean phytoplankton fluorescence intensity can be used to quantify the rate at which the electrode inhibits the chl-a fluorescence signal, for the diatoms their fluorescence intensity decreases dramatically over the course of the experiment.

The inlay of Fig. 2 plots the time at which the phytoplankton fluorescence intensity decrease is initiated as plotted against the distance squared; a clear quasi-linear correlation is recorded; such that, the time taken for the diatom fluorescence to be 'switched off' correlates directly with the distance of the

individual algal cells from the electrode. The results shown in the inlay of Fig. 2 come from three separate experiments highlighting the reproducibility of the system. Note at longer distances there is a further deviation away from this linearity, see ESI† Section 5 and 8 for further discussion and the data analysis method. From this set of experiments it is clear that the chemical products of the electro-oxidation process diffuse away from the electrode and increasingly inhibit the phytoplankton fluorescence at greater distance from the electrode with time.

An important question is; what is the identity of the electro-generated species causing the change in the phytoplankton fluorescence? Previous work in the literature has shown both *in vivo* and *in vitro* that strongly oxidising radical species, such as the hydroxyl radical, can cause the oxidative destruction of chl-a.³⁸ In this work a number of small oxidising molecules can be produced at the electrode potentials used, including, oxygen ($1.9\text{--}2.1 \times 10^{-9}\text{ m}^2\text{ s}^{-1}$),³⁹⁻⁴² chlorine ($1.38 \times 10^{-9}\text{ m}^2\text{ s}^{-1}$),⁴³ hydrogen peroxide ($1.43 \times 10^{-9}\text{ m}^2\text{ s}^{-1}$),⁴² and hydroxyl radicals ($1\text{--}3 \times 10^{-9}\text{ m}^2\text{ s}^{-1}$),^{44,45} all of which have comparable diffusion coefficients. In order to try and identify the active species the *in vivo* chl-a fluorescence spectra of a *H. coffeeaeformis* culture was studied in homogenous solution as a function of the chemical conditions (see ESI† Section 6). The fluorescence emission peak at 680 nm did not change significantly with the addition of either $0.1\text{ M HCl}_{(\text{aq})}$, H_2O_2 (33%) or $100\text{ mM FeSO}_4_{(\text{aq})}$. However, addition of H_2O_2 (33%) together with $100\text{ mM FeSO}_4_{(\text{aq})}$, (known as "Fenton's reagent") led to a significant drop in emission intensity at 680 nm . The Fe^{2+} is well known to act as a catalyst for the breakdown of H_2O_2 to generate reactive oxygen radicals *in situ*⁴⁶



Although chlorine can also lead to the oxidative destruction of the chl-a phytoplankton fluorescence signal, work provided in ESI† Section 6 demonstrates how the electrochemical inhibition may also be driven to occur in the absence of solution phase chloride. As the presence of chloride is not essential, it is therefore likely that oxidative radical species are the primary cause of the fluorescence inhibition. Furthermore, despite the fact that Fenton's reagent forms hydroxyl radicals, this species is highly reactive with a sub-micro second lifetime.⁴⁴ Consequently, since the phytoplankton are situated away from the electrochemical interface it is possible that it is the generated products from hydroxyl radical reactions²⁶ in the fluoroelectrochemical experiment that propagated away to react with the phytoplankton and are the primary cause of the observed fluorescence 'switch off'. However the direct involvement of very low OH^\cdot concentration cannot be discounted and so in summary it can be concluded, at present, that OH^\cdot or products derived from it are responsible for the switch off.

Next, we turn to consider how other phytoplankton species are affected by the oxidation process. First, the fluoroelectrochemical experiment was conducted with a cell containing the diatom *H. coffeeaeformis* (as used above), the

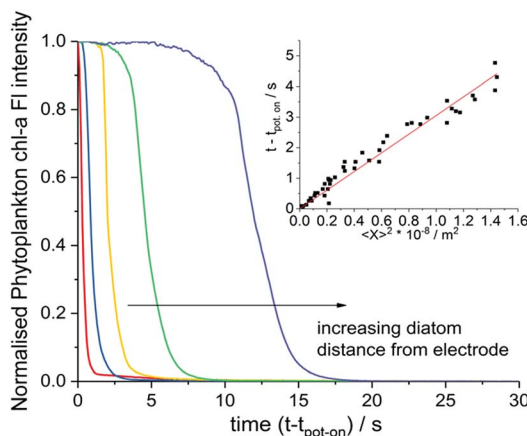


Fig. 2 Normalised chl-a fluorescence intensity of individual *H. coffeeaeformis* cells (diatom, CCAP 1001/2) located at different distances from the electrode during the fluoro-ch chronoamperometry experiment. The fluorescence intensity of the phytoplankton have been normalised relative to their intensity measured at the onset of the high overpotential application at $t - t_{\text{pot-on}} = 0.0\text{ s}$. The algal cells are located at distance of approximately $10, 30, 60, 120$ and $250\text{ }\mu\text{m}$ from the carbon electrode for the red, blue, yellow, green and purple lines respectively. Inlay shows a plot of the time taken for a diatom's chl-a fluorescence intensity to drop abnormally due to the potential step, *versus* the square of the measured perpendicular distance of the diatoms from the electrode.



coccolithophore *E. huxleyi* and the dinoflagellate *S. trochoidea*; see ESI† Section 3 for example experimental videos. Fig. 3 shows a plot of the normalised fluorescence intensity, for a representative individual *H. coffeeaeformis* and *E. huxleyi*, approximately equidistant from the electrode (*ca.* 20 μm), plotted against time after onset of the oxidising potential. First, the *H. coffeeaeformis* fluorescence (yellow line) starts to decrease only a second after the electrode potential has been switched to +2.3 V. Second, in contrast the fluorescence intensity of the *E. huxleyi* (red line) initially increases slightly but then shows a dramatic decrease in fluorescence intensity after 15 s of electrode potential being changed.

As shown in ESI† Section 7 this rapid drop in fluorescence intensity is a general feature of the *E. huxleyi* response towards the oxidative conditions. These two plankton are present in the *same* electrochemical experiment and hence the differing behaviour is not related to any variability in the electrochemical conditions. The rapid loss of fluorescence for the *E. huxleyi* after an initial delay most likely arises due to the cells outer structure being initially less permeable to the oxidative species followed by the sudden and rapid breaching of the shell, presumably caused by external chemical attack of the oxidative radical species. This conclusion is corroborated by the recorded microscope response of the *S. trochoidea* (see ESI† Section 3), this phytoplankton is relatively large compared to the others used in this study with a diameter of $>20\text{ }\mu\text{m}$. Consequently, with the use of 40X objective the internal structure of the plankton can be monitored; the experimental video (ESI† Section 3) shows that the major decrease in the phytoplankton fluorescence occurs after an abrupt change in the phytoplankton structure; which is likely associated with the rupturing of the cells external protection layer. These results are strongly suggestive that difference in behaviour of the species relates not to their size but due to their differing biomineral covering or outer membrane structures.

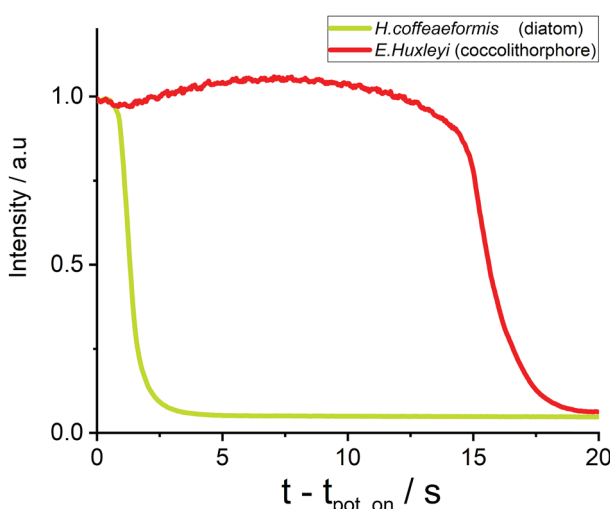


Fig. 3 Chlorophyll-a fluorescence response of diatom (*H. coffeeaeformis*, CCAP 1001/2, yellow line) and coccolithophore (*E. huxleyi*, RCC 174, red line) at equal distance $20 \pm 1\text{ }\mu\text{m}$ away from the electrode.

We turn to consider to what extent the sensitivity towards oxidative attack differs between phytoplankton groups. The fluoro-electrochemical experiment described above was undertaken with an additional four different species of phytoplankton. Fig. 4a plots the total collated results for the seven different phytoplankton species studied, here the onset of the fluorescence decrease as a function of time has been plotted against the phytoplankton distance from the electrode squared. Fig. 4a shows that, although for a given species there is a strong correlation between the distance between the electrode and the time at which the fluorescence inhibition onsets, there is a very wide difference in behaviour between the different species. For example on the time scale of this experiment, only *ca.* 24% of the *E. huxleyi* observed within the field of the microscope were affected by the oxidative potential and all of those affected were within 60 μm of the electrode. In contrast, the fluorescence signals of all of the *S. bacillaris*, within a distance of approximately 100 μm of the electrode, were inhibited within 2 seconds of the oxidising potential being applied to the electrode. Note, the dinoflagellate *S. trochoidea* was also studied within the electro-fluorescence cell. *S. trochoidea* are relatively large and present in solution at low cell densities. Hence, the imaging of only three individual *S. trochoidea* was achieved the results of which are presented in Fig. 4a – black squares. For all of the species presented in Fig. 4a – excluding *S. trochoidea*, for which insufficient data could be acquired – the scatter plot for each species is quasi-linear; the 95% confidence interval of a line of best fit is overlaid on the data.

This linearity in the plot of the square of the distance *versus* time predominantly reflects the fact that the reactive species created at the electrode need to diffuse away from the interface prior to reacting with and damaging the phytoplankton. For a molecule freely diffusing in solution, the mean square distance travelled $\langle X^2 \rangle$ in one dimension is equal to:⁴⁷

$$\langle X^2 \rangle \approx 2Dt \quad (3)$$

where D ($\text{m}^2\text{ s}^{-1}$) is the diffusion coefficient and t is time (s). Consequently, after ten seconds a molecule with a diffusion coefficient of $1 \times 10^{-9}\text{ m}^2\text{ s}^{-1}$ will have travelled on average a distance of $\sim 140\text{ }\mu\text{m}$. Such distances are comparable to those we observe optically. In Fig. 4a and using the relationship shown in eqn (3), the inverse of the gradient of the line of best fit can be used to characterise the rate at which the phytoplankton respond to the oxidative potential on the electrode. We term this inverse gradient the ‘susceptibility factor’ and it reflects the rate of mass-transport of the radical species, the used experimental conditions and the susceptibility of the plankton species towards attack from the oxidative radicals. ESI† Section 8 presents a simplified theoretical model exploring the dependency of the response time on the diffusional mass-transport rate and phytoplankton susceptibility and gives physical insight into the underlying processes. Ultimately, as the fluorescence response of the plankton are recorded under the same experimental conditions then the measured t *vs.* X^2 gradient for the different plankton can be used to give a relative measure of their susceptibility to strongly oxidising environments. Fig. 4b presents the plot of the relative susceptibility factor for the different phytoplankton,



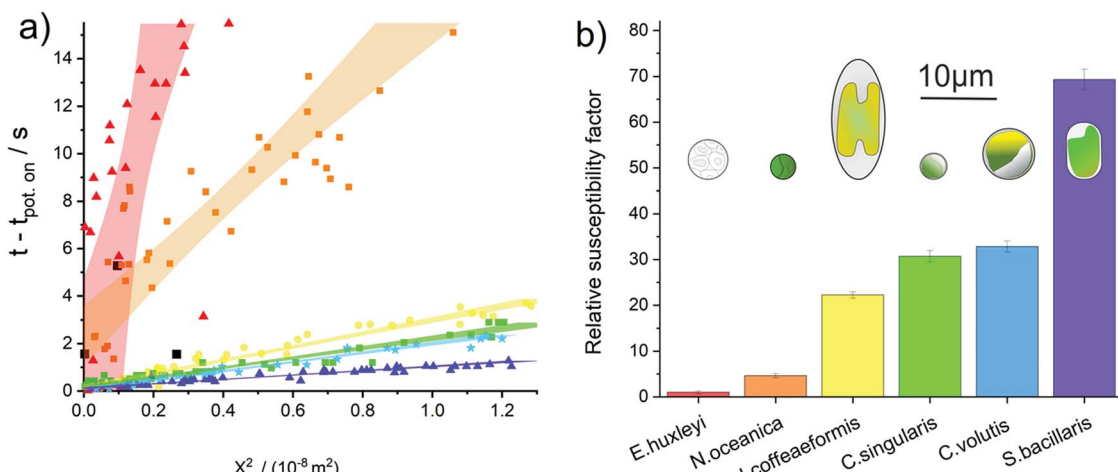


Fig. 4 (a) A plot of time at which chl-a fluorescence decrease abnormally after application of an oxidising electrode potential versus square of the distance of the phytoplankton from the electrode. Red triangles – *E. huxleyi*; orange squares – *N. oceanica*; yellow circles – *H. coffeeaeformis*; green squares – *C. singularis*; blue stars – *C. volutis*; magenta triangles – *S. bacillaris* and black squares – *S. trochoidea*. The highlighted areas depict the 95% confidence for the line of best fit as used in the calculation of the susceptibility factor, note the line of best fit has not been forced through the origin. (b) plots the relative susceptibility factor for each species towards oxidative radical attack, normalised to *E. huxleyi*. Also shown on this plot are cartoons representing the size and shape of the plankton involved, this demonstrates that there is no clear correlation between the plankton susceptibility and its morphology or size.

normalised against the measured rate for the phytoplankton most resilient to oxidative environment in this study, *E. huxleyi*. These experimental values differ by almost two orders of magnitude, such that, the least resilient and hence plankton with the highest susceptibility (*S. bacillaris*) reacts 69 ± 2 times faster than the coccolithophore *E. huxleyi*. First, the data presented in Fig. 4b does not reflect either the size or shape of the phytoplankton. Overlaid on Fig. 4b are schematic diagrams that show the approximate size and morphology of the used phytoplankton species, the diatom *H. coffeeaeformis* is the largest phytoplankton for which we have measured a relative susceptibility factor; however, its value is similar in magnitude to significantly smaller plankton. Moreover, the plankton *C. singularis* and *C. volutis*, are of the same genus and have very comparable relative susceptibility factor but they are distinctly different in size. Second, broadly the freshwater species (*C. singularis*, *C. volutis* and *S. bacillaris*) appear to be more susceptible to oxidative attack than the marine species (*E. huxleyi*, *S. trochoidea*, *N. oceanica* and *H. coffeeaeformis*). These results further corroborate the conclusion that the difference in the observed fluorescence behaviour predominantly reflects the chemical and physical characteristics of the phytoplankton shell and outer membranes. Consequently, the susceptibility of the phytoplankton towards oxidative radical attack is evidenced to be group specific and reflects the diverse structural properties of the exterior of these microscopic single cell organisms.

Conclusions

In this work the chl-a fluorescence of phytoplankton was investigated using a fluoro-electrochemical cell. The phytoplankton were found to be highly sensitive to electrochemically oxidising but not reductive conditions. The *in situ* electrochemically

generated radical species irreversibly inhibit the phytoplankton fluorescence. This inhibition rate is evidenced to reflect neither the size nor the shape of the phytoplankton but most likely relates to the physical and chemical properties of the shell and outer membrane of the phytoplankton; the rate determining step is the chemical destruction of the outer cellular structure, once the radicals enter the cell the chl-a fluorescence is rapidly extinguished. Profoundly, the rate at which the fluorescence is inhibited varies between species by almost two orders of magnitude. Beyond, possible biological implications of the differing susceptibility of different plankton group towards extreme oxidative stress, on a pragmatic level the ability to differentiate between phytoplankton on the basis of their oxidative susceptibility has potential application in high-throughput methods for phytoplankton identification and bloom monitoring.

Conflicts of interest

There are no conflicts to declare.

Acknowledgements

This research was partially funded by St. John's College Oxford. This project has also received funding from the European Research Council (ERC) under the European Union's Horizon 2020 research and innovation programme (APPELS project, grant agreement 681746).

Notes and references

- 1 A. Sournia, M. J. Chrdtiennot-Dinet and M. Ricard, *J. Plankton Res.*, 1991, **13**, 1093–1099.

2 J. R. Reinfelder, *Annual Review of Marine Science*, 2011, **3**, 291–315.

3 D. G. Boyce, M. R. Lewis and B. Worm, *Nature*, 2010, **466**, 591.

4 D. G. Boyce, M. Dowd, M. R. Lewis and B. Worm, *Prog. Oceanogr.*, 2014, **122**, 163–173.

5 H. Claustre and S. Maritorena, *Science*, 2003, **302**, 1514–1515.

6 D. Blondeau-Patissier, J. F. Gower, A. G. Dekker, S. R. Phinn and V. E. Brando, *Prog. Oceanogr.*, 2014, **123**, 123–144.

7 B. B. Barnes, C. Hu, B. A. Schaeffer, Z. Lee, D. A. Palandro and J. C. Lehrter, *Remote Sensing of Environment*, 2013, **134**, 377–391.

8 A. Nair, S. Sathyendranath, T. Platt, J. Morales, V. Stuart, M.-H. Forget, E. Devred and H. Bouman, *Remote Sensing of Environment*, 2008, **112**, 3366–3375.

9 A. D. Jassby and T. Platt, *Limnol. Oceanogr.*, 1976, **21**, 540–547.

10 M. A. Marcoval, V. E. Villafane and E. W. Helbling, *J. Photochem. Photobiol. B*, 2007, **89**, 78–87.

11 M. Y. Gorbunov, Z. S. Kolber and P. G. Falkowski, *Photosynth. Res.*, 1999, **62**, 141–153.

12 V. Randhawa, M. Thakkar and L. Wei, *Aquat. Toxicol.*, 2013, **142**, 230–238.

13 J. L. Collier, *J. Phycol.*, 2000, **36**, 628–644.

14 R. Jonker, R. Groben, G. Tarran, L. Medlin, M. Wilkins, L. García, L. Zabala and L. Boddy, *Sci. Mar.*, 2000, **64**, 225–234.

15 U. Riebesell, I. Zondervan, B. Rost, P. D. Tortell, R. E. Zeebe and F. M. Morel, *Nature*, 2000, **407**, 364.

16 D. A. Wolf-Gladrow, U. Riebesell, S. Burkhardt and J. Bijma, *Tellus B*, 1999, **51**, 461–476.

17 J. C. Orr, V. J. Fabry, O. Aumont, L. Bopp, S. C. Doney, R. A. Feely, A. Gnanadesikan, N. Gruber, A. Ishida and F. Joos, *Nature*, 2005, **437**, 681.

18 J. C. Steinmetz, in *Coccolithophores*, Cambridge University Press, Cambridge, 1994, pp. 179–197.

19 T. Anning, N. Nimer, M. Merrett and C. Brownlee, *Journal of Marine Systems*, 1996, **9**, 45–56.

20 F. M. Monteiro, L. T. Bach, C. Brownlee, P. Bown, R. E. Rickaby, A. J. Poulton, T. Tyrrell, L. Beaufort, S. Dutkiewicz and S. Gibbs, *Sci. Adv.*, 2016, **2**, e1501822.

21 U. Riebesell, *J. Oceanogr.*, 2004, **60**, 719–729.

22 E. M. Fleischmann, *Limnol. Oceanogr.*, 1989, **34**, 1623–1629.

23 J. T. O. Kirk, *Light and Photosynthesis in Aquatic Ecosystems*, Cambridge University Press, 1994.

24 N. Marbà, C. M. Duarte and S. Agustí, *Proc. Natl. Acad. Sci. U. S. A.*, 2007, **104**, 15777–15780.

25 M. Llabrés and S. Agustí, *Limnol. Oceanogr.*, 2006, **51**, 21–29.

26 S. Gligorovski, R. Strekowski, S. Barbati and D. Vione, *Chem. Rev.*, 2015, **115**, 13051–13092.

27 M. Llabrés, J. Dachs and S. Agustí, *Photochem. Photobiol.*, 2012, **88**, 1473–1479.

28 K. Mopper and X. Zhou, *Science*, 1990, **250**, 661–664.

29 M. Bai, Z. Zhang, N. Zhang, Y. Tian, C. Chen and X. Meng, *Plasma Chem. Plasma Process.*, 2012, **32**, 693–702.

30 M. Bai, Z. Zhang, X. Xue, X. Yang, L. Hua and D. Fan, *Plasma Chem. Plasma Process.*, 2010, **30**, 831–840.

31 Y. Zhang, M. Bai, C. Chen, X. Meng, Y. Tian, N. Zhang and Z. Yu, *Plasma Chem. Plasma Process.*, 2013, **33**, 751–763.

32 Z. Zhang, M. Bai, B. Yang and X. Bai, *IEEE Trans. Plasma Sci.*, 2006, **34**, 2618–2623.

33 Z. Zhitao, B. Mindong, Y. Bo, B. Mindi and B. Xiya, *Plasma Sci. Technol.*, 2005, **7**, 3025.

34 Y. Matsumoto and E. Sato, *Mater. Chem. Phys.*, 1986, **14**, 397–426.

35 J. Rossmeisl, Z.-W. Qu, H. Zhu, G.-J. Kroes and J. K. Nørskov, *J. Electroanal. Chem.*, 2007, **607**, 83–89.

36 A. Hickling and S. Hill, *Trans. Faraday Soc.*, 1950, **46**, 557–559.

37 M. E. Abdelsalam, G. Denuault, M. A. Baldo and S. Daniele, *J. Electroanal. Chem.*, 1998, **449**, 5–7.

38 J. R. Harbour and J. R. Bolton, *Photochem. Photobiol.*, 1978, **28**, 231–234.

39 J. Jordan, E. Ackerman and R. L. Berger, *J. Am. Chem. Soc.*, 1956, **78**, 2979–2983.

40 R. E. Davis, G. L. Horvath and C. W. Tobias, *Electrochim. Acta*, 1967, **12**, 287–297.

41 D. M. Himmelblau, *Chem. Rev.*, 1964, **64**, 527–550.

42 S. A. M. van Stroe-Biezen, F. M. Everaerts, L. J. J. Janssen and R. A. Tacken, *Anal. Chim. Acta*, 1993, **273**, 553–560.

43 A. Tang and O. C. Sandall, *J. Chem. Eng. Data*, 1985, **30**, 189–191.

44 G. V. Buxton, C. L. Greenstock, W. P. Helman and A. B. Ross, *J. Phys. Chem. Ref. Data*, 1988, **17**, 513–886.

45 D. T. Kallikragas, A. Y. Plugatyr and I. M. Svishchev, *J. Chem. Eng. Data*, 2014, **59**, 1964–1969.

46 H. J. H. Fenton, *J. Chem. Soc., Trans.*, 1894, **65**, 899–910.

47 A. Einstein, *Ann. Phys.*, 1905, **322**, 549–560.

